1

Can label or protein deuteration extend the phase relaxation time of Gd(III) spin labels?

Elena Edinach[1#], Xing Zhang[2#], Chao-Yu Cui[2], Yin Yang[2], George Mitrikas[3], Alexey Bogdanov[1], Xun-Cheng Su[2,*], and Daniella Goldfarb[1,*]

[1]Department of Chemical and Biological Physics, Weizmann Institute of Science,76100 Rehovot, Israel

[2]State Key Laboratory of Elemento-Organic Chemistry, College of Chemistry, Nankai University, 300071 Tianjin, China

[3]Institute of Nanoscience and Nanotechnology, NCSR Demokritos, Athens 15310, Greece

Corresponding authors : Xun-Cheng Su, xunchengsu@nankai.edu.cn, Daniella Goldfarb, Daniella.goldfarb@weizmann.ac.il

[#] Equal contributions

15

1   **Abstract**

2   Pulse-dipolar electron paramagnetic resonance (PD-EPR) has emerged as an effective tool in

3   structural biology, enabling distance measurements between spin labels attached to

4   biomolecules. The sensitivity and the accessible distance range of these measurements are

5   governed by the phase memory time (T_m) of the spin labels. Understanding the decoherence

6   mechanisms affecting T_m is crucial for optimizing sample preparation and spin-label design. This

7   study investigates the phase relaxation behavior of two Gd(III) spin-label complexes, Gd-PyMTA

8   and Gd-TPMTA, with various degrees of deuteration. These two complexes have significantly

9   different zero-field splitting (ZFS) parameters. Hahn echo decay and dynamical decoupling (DD)

10   measurements were performed at W-band (95 GHz) in deuterated solvents (D_2O/glycerol-d_8),

11   both for the free complexes and when conjugated to proteins. The impact of temperature,

12   concentration, and field position within the EPR spectrum on T_m was examined. Results indicate

13   that protons within 5 Å of the Gd(III) ion do not contribute to nuclear spin diffusion (NSD), and

14   protein deuteration offers minimal enhancement in T_m. The dominant phase relaxation

15   mechanisms identified at low concentrations were direct spin-lattice relaxation (T_1) and transient

16   ZFS fluctuations (tZFS). Dynamical decoupling (DD) measurements, using the Carr-Purcel

17   sequence with ~140 refocusing pulses, resolved the presence of two populations: one with a long

18   phase relaxation time, $T_{m,s}$, and the other with a short one, $T_{m,f}$. The dominating mechanism for

19   the slowly relaxing population is direct-T_1. $T_{m,s}$ showed no concentration dependence and was

20   longer by a factor of about 2 from T_m for both complexes. We tentatively assign the increase in

21   $T_{m,s}$ to full suppression of the residual indirect T_1-induced NSD mechanism. For the fast relaxing

22   population, $T_{m,f}$ is shorter for Gd-TPMTA; therefore, we assign it to populations for which the tZFS

23   mechanism dominates. Because of the relatively short T_1 and the contribution of tZFS mechanism,

24   protein deuteration does not significantly affect T_m.

25

1   1.   Introduction

2   Distance measurements between two spin labels attached at specific sites in biomolecules,

3   determined by pulse-dipolar EPR (PD-EPR) methods, have become standard tools in structural

4   biology. The sensitivity of these measurements and the distance they can access depend on the

5   phase memory time, T_m, of the spin labels used. Accordingly, understanding the decoherence

6   mechanisms is essential for optimizing sample preparation conditions (concentrations, solvent

7   composition, deuteration) and for spin-label design, thus reaching as long as possible T_m. In the

8   case of solid-state EPR where the pulses applied cannot excite the entire width of the EPR

9   spectrum, the spins are commonly divided into two types: Those excited and observed by the

10   microwave pulse are referred to as the "A" spins, and the rest, termed "B" spins, are much more

11   abundant. In general, at low temperatures, at which PD-EPR experiments are commonly carried

12   out, there is no motion and the mechanisms contributing to decoherence for spin labels with

13   S=1/2 are (Salikhov et al., 1981; Tyryshkin et al., 2012; Mitrikas, 2023; Wilson et al., 2023; Eaton

14   and Eaton, 2000): (i) Direct spin-lattice (T_1) relaxation mechanism of the A spins, $T_{m,T1}$, which

15   provides the highest limit $T_m \leq 2T_1$.(ii) Redistribution of resonance frequencies of dipole-

16   coupled A spins due to mw pulses leads to instantaneous diffusion, ID. (iii) Coupling between A

17   spins and nearby B spins leads to spectral diffusion, SD. The latter can result from T_1 flips of the

18   coupled B spins, referred to as indirect-T_1, SD-T_1, or energy-conserving pairwise B spin flip-flops,

19   SD-ee. All these are concentration dependent. (iv) Nuclear spin diffusion (NSD) arising from

20   nuclear flip-flops caused by homonuclear couplings, which does not depend on the electron spin

21   concentration but depends on the nuclei concentration. (v) Admixture of tunnel states of methyl

22   groups into the electron spin mediated by the hyperfine coupling of methyl protons (Soetbeer et

23   al., 2021a).

24   Gd(III) chelates are among the spin labels used for PD-EPR applications; they are beneficial for in-

25   cell PD-EPR measurements because of their chemical stability and high sensitivity at high

26   frequencies (> 34 GHz, Q- and W-band) owing to a narrow central transition and a relatively long

27   phase memory time (Goldfarb, 2014; Giannoulis et al., 2021). Several studies have been dedicated

28   to the dephasing mechanism of Gd(III) at low temperatures. Raitsimring et al (Raitsimring et al.,

29   2014) explored the phase relaxation of Gd(III)-DOTA as a representative of Gd(III) spin labels in

30   the temperature and concentration ranges typically used for W-band double electron-electron

31   (DEER) measurements, which is the most widely applied PD-EPR experiment (Pannier et al., 2000).

They found that in addition to the mechanisms of phase relaxation known for nitroxide-based spin labels listed above, Gd(III) spin labels are subjected to an additional phase relaxation mechanism that features an increase in the relaxation rate from the center to the periphery of the EPR spectrum. It was suggested that this mechanism is due to transient zero-field splitting (tZFS) fluctuations. This tZFS-induced phase relaxation mechanism becomes dominant (or at least significant) when all other phase relaxation mechanisms mentioned above are significantly suppressed by matrix (solvent) deuteration and low spin concentration.

A quantitative analysis of Gd(III) Hahn echo decay was recently reported at 240 GHz (Wilson et al., 2023). Two complexes, Gd-DOTA (D=700 MHz) and Gd-PyMTA (D=1200 MHz), were studied in D_2O/glycerol-d_8. T_1 and T_m were measured as a function of temperature and concentration. As expected, T_1 was found to be concentration-independent, whereas T_m was. Interestingly, the Hahn echo decay from which T_m was derived could be fitted by an exponential decay instead of the stretched exponent needed at Q-band (Soetbeer et al., 2021b). A careful analysis of the temperature and concentration dependence data and the associated T_1 values gave the relative contributions of the various decoherence mechanisms. The concentration-independent mechanism was found to be the direct-T_1 mechanism and a concentration- and temperature-independent mechanism was assigned to weak coupling between electron spins and the presence of an ensemble of nuclear spins. As the solvent was fully deuterated, these could be protons on the Gd(III) complex. In this respect, it has been shown that while deuteration of nitroxides spin labels did not increase T_m, for trityl labels, it did (Soetbeer et al., 2021b).

Qualitative studies of several Gd(III) complexes, with axial parameters, $D,$ of the ZFS in the range of 560-2000 MHz, investigated the effect of solvent deuteration at Q-band(Garbuio et al., 2015), and reported that in a protonated matrix, T_m is dominated by NSD. It was also suggested that in fully deuterated solvents, the phase relaxation is dominated by tZFS and perhaps ligand hyperfine-driven mechanism, but no quantitative analysis of the data was presented. The decoherence behavior of Gd(III) complexes was further investigated under dynamical decoupling (DD) conditions. DD is a control strategy to protect quantum states from decoherence, achieved by applying a sequence of carefully designed control pulses that counteract unwanted interactions with the environment, effectively "decoupling" the system from environmental noise(Suter and Álvarez, 2016). CP (Carr-Purcell) and CPMG (Carr-Purcell-Meiboom-Gill) echo trains are such sequences. DD acts as a filter between the spin system and the environment, and the pulse

spacing determines the characteristics of this filter. Short delays compared to the correlation time of the environmental fluctuations increase the coherence time of the system and typically, relaxation caused by electron-electron spectral diffusion and NSD can be suppressed (Soetbeer et al., 2021b; Soetbeer et al., 2018). Recent measurements on a single crystal of Gd(III) doped Y(trensal) carried out at X-band frequencies showed that CPMG with 120 refocusing pulses suppressed NSD efficiently and increased T_m considerably, depending on the transition probed and the crystal orientation (Hansen et al., 2024).

Three Gd(III) complexes with D values of 485-1861 MHz were studied at Q-band in protonated and deuterated solvent, H_2O/glycerol and D_2O/glycerol-d_8, and a low concentration to suppress the ID and SD mechanisms (Soetbeer et al., 2021b). As expected, the solvent deuteration increased the decay time considerably, and the data could be well-fitted with a single stretched exponential decay function (SE model). Furthermore, for Gd-DOTA-M in deuterated solvents, DD (CP with up to 5 refocusing pulses) did not generate a significant increase in the decay time, and it was suggested that coherence losses of unknown origin, probably the ZFS-driven mechanism, which the DD cannot refocus, counteracted the decoupling efforts(Soetbeer et al., 2021b). Interestingly, measurements of a protein singly spin-labeled with Gd-DOTA-M in a deuterated solvent increased the echo decay rate approximately threefold, as compared to the bare spin-label in the same solvent. This three-fold increase could be counteracted by DD with 2-3 pulses, achieving overall longer coherence survival than any DD trace of the fully protonated sample (Soetbeer et al., 2021b). These results showed that the protein's protons affect the phase relaxation of the Gd(III) spin label. Thus, one would expect that deuteration of the protein should help reduce the decoherence.

The T_1 values of Gd(III) complexes in solution are relatively short and therefore expected to affect the Gd(III) phase relaxation. For example, Gd(III) ruler with a PyMTA chelate with distances of 3.4 nm have at W-band T_1 values in the range of 80-11 μs at the temperature range of 6-30 K, respectively, (Seal et al., 2022), (Razzaghi et al., 2014). For the same type of ruler with distances of 2.1 and 6 nm, a T_1 value of ~30 μs was reported at 10 K (Mocanu et al., 2025). The reported T_1 values of the spin label BrPsPy-DO3A-Gd(III) in the temperature range of 6-40 K are 132-9 μs (Seal et al., 2022). At Q-band, the T_1 values are longer than at W-band; the complexes of the [GdIII(NO3Pic)] family, which have a small ZFS D~500 MHz and T_1 values in the range of 190-200 μs, were reported (Ossadnik et al., 2023).

1   In the present work, we explore whether deuteration of the Gd(III) chelate and the protein can
2   further extend T_m, along with the effects of concentrations, temperature, and field position within
3   the Gd(III) EPR spectrum. This is done for Hahn echo decay measurements, and the potential of
4   DD for extending it further is also examined. We studied two Gd(III) spin-label complexes, PyMTA
5   (Gd-PyMTA) and TPMTA (Gd-TPMTA) (**Fig. 1**), with different degrees of deuteration. These two
6   complexes have very different D values (1200 vs ~4000 MHz). All measurements were carried out
7   at W-band (95 GHz), and the complexes were dissolved in D_2O/glycerol-d_8, thus serving as a
8   reference for the longest possible T_m. These are then compared to the phase relaxation of these
9   labels when conjugated to a protein. We found that the protons at a distance shorter than 5 Å
10 from the Gd(III) do not contribute to NSD and that the protein's deuteration did not significantly
11 prolong T_m. The primary mechanisms contributing to the phase relaxation in deuterated solvents
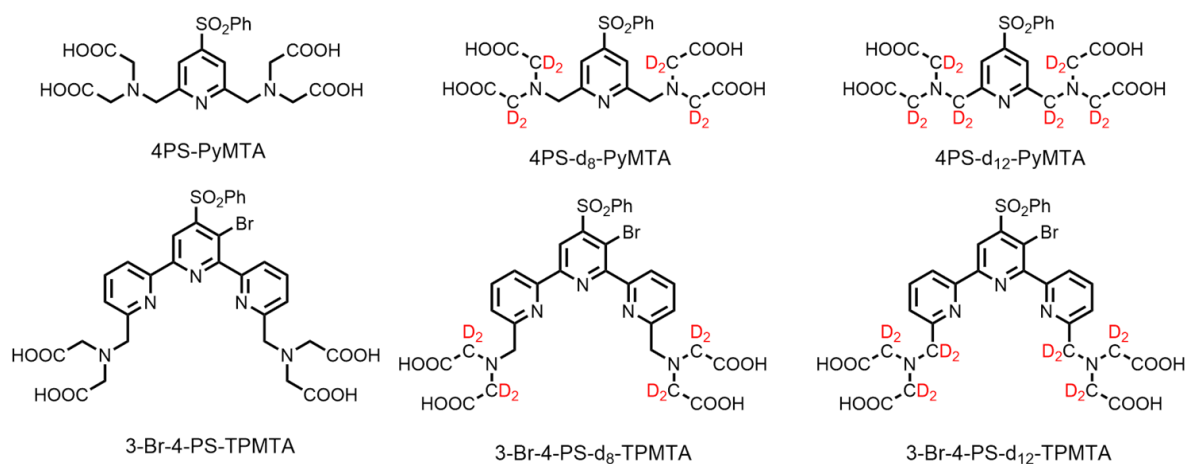12 and low concentrations are the direct T_1 and tZFS mechanisms.

13

14 *Figure 1. Deuterated chelates for Gd(III) that can be further attached to cysteine residues in a*
15 *protein for labeling.*

16 **1.   Experimental**

17 1.1 Synthesis of spin labels

18 The synthesis of spin tags, protein expression and labeling are described in detail in the Supporting
19 Information. In brief, the 4PS-(d_n)-PyMTA were synthesized according to reported procedure
20 (Montgomery et al., 2017; Wang et al., 2019) (Li and Byrd, 2022)' (Yang et al., 2015) and 3-Br-4-
21 PS-(d_n)-TPMTA tags were synthesized in the following 8 steps (Scheme 1). 1: Methylation of (3-1)
22 with CH_3I and K_2CO_3 in acetone, purification via column chromatography (82% yield). 2:
23 Bromination of (3-2) with N-Bromusuccinimide (NBS) in acetic acid at 60 °C, and chromatography

1   purification (92% yield). 3: Reduction of (3-3) with $NaBH_4$/$NaBD_4$ in ethanol, yielding a yellow solid.

2   4: Reaction of (3-4) with PBr_3 in $CHCl_3$, followed by neutralization and extraction. 5: Substitution

3   of (3-5) with diethyl iminodiacetate in acetonitrile at 70 °C, yielding a yellow solid. 6: Reaction of

4   (3-6) with $POBr_3$ in DMF at 105 °C and purification. 7: Reaction of (3-7) with sodium benzene

5   sulfinate and TBAB in acetonitrile at 90 °C. 8: Hydrolysis of (3-8) with NaOH/NaOD in THF/H_2O,

6   followed by acidification, resulting in (3-9) as a yellow solid. The synthesis of 4PS-5-Br-6PCA-(d_n)-

7   DO3A-Gd(III) is described in detail in the Supporting Information. Mass spectra of all tags are given

8   in **Figs. S1-S3**.
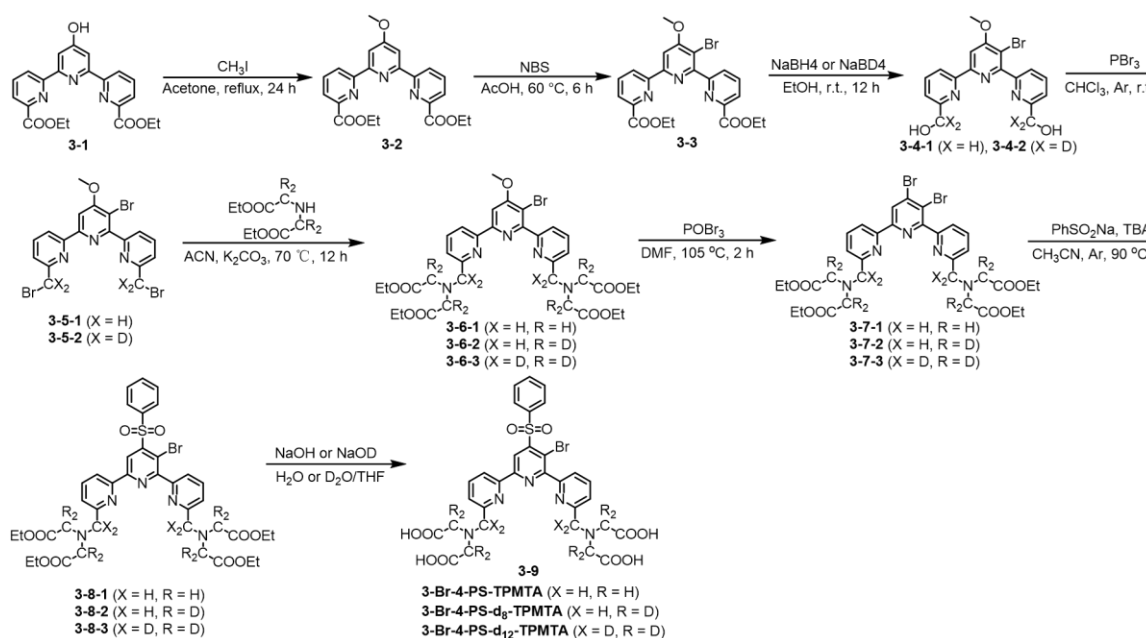
Scheme 1. *Synthesis of 3-Br-4-PS-(d_n)-TPMTA spin tags.*

9

10   <u>2.2 Protein purification, spin labeling, and EPR sample preparation</u>

11   The D39C/E64C construct of ubiquitin (ubi) was used in this study. The steps for deuterated

12   protein expression were performed according to previous reports (Li and Byrd, 2022).

13   *2.2.1   Protein labeling with 4PS-5-Br-6PCA-(d_n)-DO3A-Gd(III).*

14   0.2 mM 100 µL purified protein ([1]H ^{14}N ubi D39C/E64C or [2]H ^{15}N ubi D39C/E64C) was incubated

15   with 0.4 mM tris(2-carboxyethyl)phosphine (TCEP) in 20 mM Tris-HCl at pH 8.5, and then treated

16   with 10 equivalents of tags at 30 °C for 12 h. The reaction progress was monitored by ESI-Q-TOF

17   mass spectrometry. The excess tag was removed using a PD-10 desalting column (GE Healthcare

18   Biosciences). The ligation products were freeze-dried for subsequent experiments.

1 *2.2.3   Protein labeling with 4PS-PyMTA or 3-Br-4PS-TPMTA.*

2 The ligation of the target protein to 4PS-PyMTA was carried out according to the previous report

3 (Yang et al., 2019). 0.2 mM 100 µL purified protein in 20 mM Tris-HCl at pH 8.5 was mixed with

4 0.4 mM TCEP, and then treated with 10 equivalents tags at 30 °C for 12 h. After the reaction was

5 completed, the sample was filtered through PD-10 desalting column to remove the excess tag.

6 The protein-PyMTA was mixed with 2.5 equivalents of $Gd(NO_3)_3$ in a 20 mM MES buffer at pH 6.5.

7 The excess of metal ion was removed using a Millipore concentrator (3 kDa cutoff). Similarly, 3-

8 Br-4PS-TPMTA was conjugated to the target protein using the same procedure, and the

9 deuterated tags were ligated to the target protein the same as the non-deuterated tag. Mass-

10 spectra of the labeled proteins are shown in **Figs. S4-S7**.

11 For pulse EPR measurements, Gd-PyMTA and Gd-TPMTA solutions in the concentration range of

12 0.03-0.2 mM were dissolved in 50:50 v/v D_2O/glycerol-d_8. The spin-labeled protein conjugates

13 were lyophilized and redissolved in 15 mM HEPES-D_2O buffer (pD 7.2) with 20% glycerol-d_8 (v:v).

14 The final concentration of proteins was 50 µM estimated from the absorbance at 280 nm using a

15 Nanodrop spectrophotometer (Thermo Science). For EPR measurements, solutions (ca. 3 µL) were

16 transferred to quartz capillaries (0.6 ID × 0.84 OD mm) and sealed at one end with crytoseal.

17 *2.3   Spectroscopic measurements*

18 Pulsed EPR and ENDOR measurements were performed using two home-built W-band pulse EPR

19 spectrometers equipped with cylindrical TE_{011} cavities and Helmholtz radiofrequency (RF) coils

20 (Gromov et al., 1999). The first spectrometer has a solenoid superconducting magnet

21 (Cryomagnetics, Inc.), a 3 W pulsed microwave power amplifier (QPP95013530, Quinstar), and a

22 pulsed 2 kW RF amplifier (BT02000-GammaS, TOMCO). The second spectrometer has a 0–5 T

23 cryogen-free magnet with an integrated variable temperature unit and 300 mT sweep coil (J3678,

24 Cryogenic Ltd.)(Feintuch et al., 2011), and is equipped with 2 W pulsed microwave power

25 amplifier (QPP95023330-ZW1, Quinstar). Temperature (below 15 K) and field dependencies of Gd

26 -TPMTA were carried out using the second spectrometer due to its wide temperature and

27 magnetic field ranges.

28 Echo-detected EPR (ED-EPR) spectra were recorded employing the Hahn echo sequence ($\pi/2-\tau-$

29 $\pi-\tau-$echo) and measuring the echo intensity as a function of the magnetic field. The π pulse

30 duration was 28-30 ns, τ=500-600 ns, and a repetition time of 1 ms was employed. Echo decays

31 as a function of τ were measured by setting the magnetic field to a position within the ED-EPR

32 spectrum and the experimental parameters described above. The Carr–Purcell (CP) experiments

1   were carried out using the $\pi/2 - (\tau/n - \pi - \tau/n)_n$ – echo sequence with a 2^n-step phase cycle

2   employed to filter out all additional echoes except the refocused ones (Soetbeer et al., 2018). For

3   these experiments, n was from 1 to 5 with varying τ for each value of n and measuring the intensity

4   of the last echo as a function of τ. Additionally, a full CP train $\pi/2_x - (\tau - \pi_x - \tau - echo - \tau - \pi_{-x} - \tau$

5    $- echo)_n$ (Mentink-Vigier et al., 2013) was applied with a two-step phase cycling on the first $\pi/2$

6   pulse, with constant τ in the range of 280 to 800 ns and the intensity of each echo was measured,

7   typically 2n~140. T_1 measurements were performed using the inversion recovery sequence, $\pi -$

8    $t_{wait} - \pi/2 - \tau - \pi - \tau - echo$, with varying t_{wait}.

9   Mims ENDOR spectra were recorded on the first spectrometer at 10-20 K and a magnetic field

10   corresponding to maximum echo intensity using the sequence $\pi/2–\tau–\pi/2–T(\pi_{RF})–\pi/2–\tau–echo–$

11    $[\tau_2–\pi–\tau_2–echo]_n$ with a four-step phase cycle and five CP echoes with $\tau_2 = 600$ ns for detection,

12   which was optimized for the best signal-to-noise ratio (Mentink-Vigier et al., 2013). The RF

13   frequency was varied randomly (Epel et al., 2003). The experimental parameters for the Mims

14   ENDOR spectra were T=42 µs, τ varied from 280 ns to 600 ns. RF power was adjusted to yield the

15   desired π_{RF} pulse length (40 µs) using a Rabi nutation sequence, $\pi/2–\tau–\pi/2–T(t_{RF})–\pi/2–\tau–echo$,

16   with a constant mixing time, T, of 100 µs and varying RF pulse length, t_{RF}.

17   2.4. Simulations of the ED-EPR spectra:

18   ED-EPR spectra were simulated using solid-state simulation function "pepper" of the EasySpin

19   program package (version 6.0.0-dev.50) (Stoll and Schweiger, 2006).. The distributions of ZFS

20   parameters were considered using a built-in EasySpin functionality (DStrain parameter; the

21   distributions in E and D were treated as uncorrelated), and the Boltzmann thermal polarization of

22   the electron spin levels at W-band at the temperature of the experiment was taken into account.

23   A Gaussian line shape with 0.1 mT width was used in the simulations. To account for the

24   differences in turning angles for different electron spin manifolds in a pulsed ED-EPR experiment,

25   intensities of individual transitions $\left|m_S\right\rangle \leftrightarrow \left|m_S+1\right\rangle$ were renormalized according to

26    $\sin^3\left(\pi\alpha/2\right)\cdot\alpha^{-1}$ (Raitsimring   et   al.,   2013)   where

27    $\alpha = \sqrt{S(S+1)-m_S(m_S+1)}\Big/\sqrt{S(S+1)+0.25}$ and $S=7/2$. This approach still does not

28   consider the difference in phase memory times of different electron spin manifolds, which is

29   minor for the short inter-pulse τ delays used in the ED-EPR sequence (500–600 ns). The optimal

30   values of the parameters were determined by non-linear least-squares fitting.

31

1   **3. Results and discussion**

2   3.1 Deuterated Gd(III) spin labels

3   *3.1.1 ED-EPR and ENDOR spectra*

4   Before proceeding with the relaxation measurements, we carried out spectroscopic

5   characterizations of the samples. The W-band echo detected EPR (ED-EPR) spectra of Gd-PyMTA

6   and Gd-TPMTA, recorded at 10 K, are shown in **Fig. 2A,B**. The spectrum of Gd-PyMTA is typical for

7   Gd(III) spin labels with a moderate ZFS (D=1200 MHz)[27] in frozen solutions where the m_S=-1/2 to

8   m_S=1/2 central transition (CT) dominates and appears as an intense peak superimposed on a

9   broad featureless background, arising from all other transitions. The unresolved broad

10 background results from a large distribution in the ZFS parameters D and E(Raitsimring et al.,

11 2005). The spectrum of Gd-TPMTA is unusual; the central transition has a fine structure, and the

12 broad background on which it is superimposed has clear singularities. This indicates that the ZFS

13 is considerably larger than for Gd-PyMTA and that the distributions of D and E are smaller. To ease

14 the assignment of the various features of the spectrum, we recorded the spectrum at lower

15 temperatures, where the contribution of the CT decreases and those of the low-lying transitions

16 |-7/2>$\rightarrow$|-5/2> and |-5/2>$\rightarrow$|-3/2> increase. The spectra are presented in **Fig. 2C** with the

17 annotation of the powder pattern's x, y, and z singularities corresponding to the various

18 transitions. Simulations of the spectra presented in **Fig. 2D** gave D=4200 MHz, ΔD=390 MHz,

19 E=440 MHz, and ΔE=370 MHz. We attribute the larger ZFS values and the smaller distributions to

20 TPMTA offering optimal 9 coordination sites for Gd(III), and holding it in a well-defined position.

21 This is in contrast to to PyMTA, which has 7 coordination sites, and the other two are
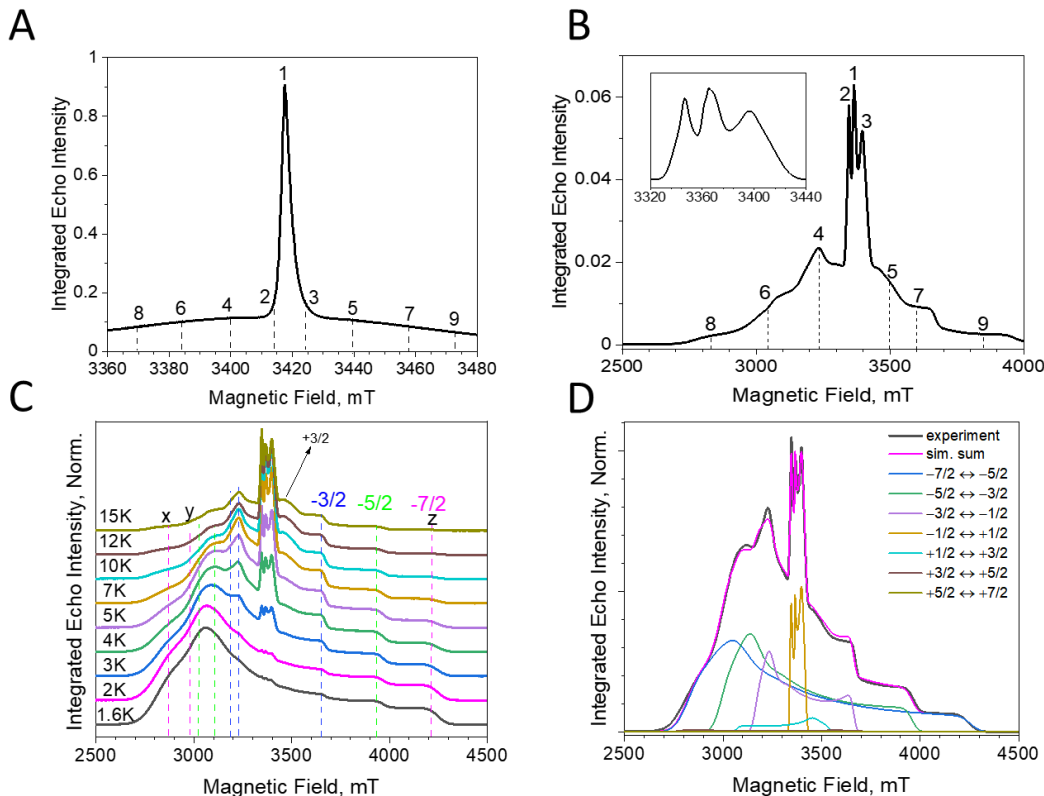
22 supplemented by water molecules.

Figure 2. ED-EPR spectra (10 K) of Gd-PyMTA (A) and Gd-TPMTA (B). The central transition of Gd-TPMTA is shown in the insert on the right with an extended scale. The different numbers indicate positions at which relaxation measurements took place. C) Temperature-dependent ED-EPR spectra of Gd-TPMTA. The positions of the x,y,z singularities of the powder patterns of the various transitions are indicated by dashed lines according to the color code: blue for -3/2 →-1/2, green for -5/2 →-3/2 and magenta for -7/2 →-5/2 . D) Simulations of the spectrum in (C) recorded at 5 K, the simulation parameters are given in the text.

Next, we carried out W-band Mims ENDOR measurements to test the efficiency of the deuteration and determine the hyperfine couplings of the different protons, which are important for identifying their potential contributions to decoherence by NSD. **Fig. 3A,B** presents the spectra of Gd-PyMTA, Gd-PyMTA-d$_8$, and Gd-PyMTA-d$_{12}$ measured with τ=280 ns to highlight the large ^{1}H couplings and τ=600 ns to highlight the small ^{1}H couplings.

For Gd-PyMTA-d$_{12}$ the spectrum is dominated by the protons on the pyridine ring, having a coupling a$_\perp$=440 kHz, and the protons on the phenyl ring with a$_\perp$=140-170 kHz, where $a_\perp$ is the principal, perpendicular component of hyperfine tensor. A comparison of the spectra of the three Gd-PyMTA samples shows some residual methylene protons. The ENDOR spectra of Gd-TPMTA, Gd-TPMTA-d$_8$, and Gd-TPMTA-d$_{12}$ are presented in **Fig. 4C,D**. In this case, the remaining protons of Gd-TPMTA-d$_{12}$ are situated on three pyridine rings and are located 5.5 and 6.5-7 Å away from

1   the Gd(III) with $a_\perp$=170-440 kHz. Here, the deuteration efficiency was higher than that of Gd-

2   PyMTA-d$_{12}$, as we did not observe a significant contribution of residual methylene protons. A

3   summary of the hyperfine couplings of the various protons in Gd-PyMTA and Gd-TPMTA is given
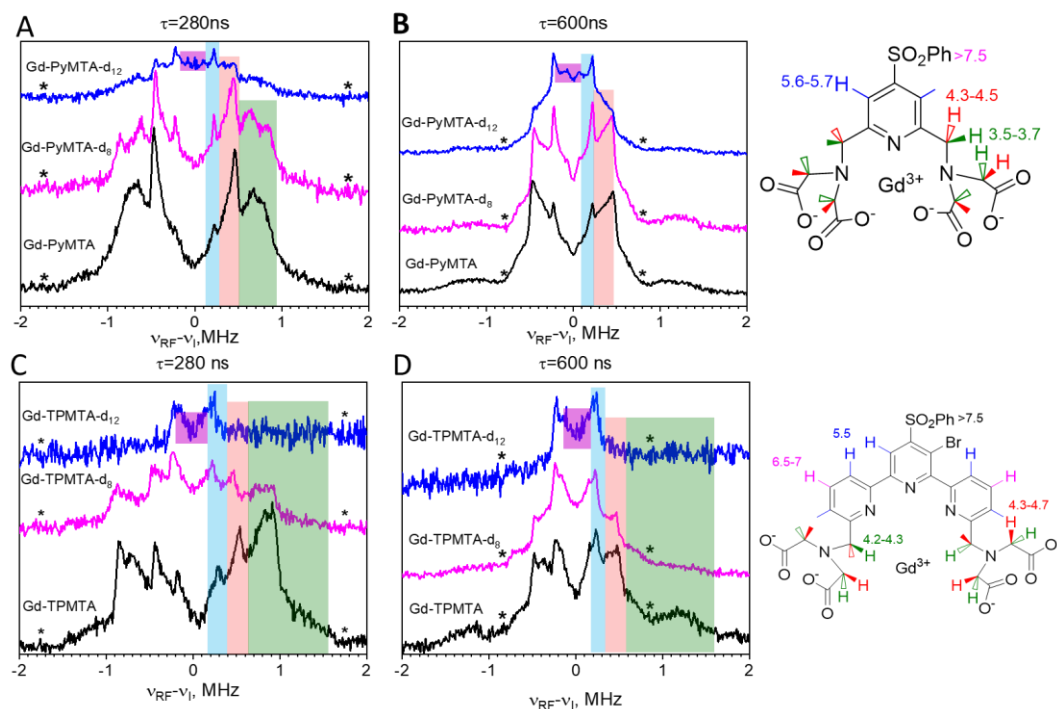
4   in **Table S1**.

5

6   *Figure 3. (A,B) Mims ENDOR spectra of Gd-PyMTA, Gd-PyMTA-d$_8$ and Gd-PyMTA-d$_{12}$ measured at*
7   *the CT with two τ values (indicated on the figure). (C,D) Mims ENDOR spectra of Gd-TPMTA, Gd-*
8   *TPMTA-d$_8$, and Gd-TPMTA-d$_{12}$, measured at the low field peak of the CT, (3381 mT) with two τ*
9   *values (indicated in the figure). The assignment of the signals is given by the colored stripes added*
10   *to the spectra following the color code given on the complex structure shown on the right. The*
11   *numbers next to the protons give the distances in Å extracted from the ENDOR doublets' splitting*
12   *under the assumption of purely dipolar couplings. The asterisks mark the position of the blind*
13   *spots.*

14   *3.1.2 Hahn echo decays*

15   Hahn echo decays were measured for all samples and could be well-fitted with a single stretched

16   exponential decay function (SE model) (eq. 1) :

17   $$y = A * exp\left[-\left(\frac{2\tau}{T_m}\right)^\beta\right] \qquad (1)$$

18   For Gd-PyMTA, measurements were carried out in the range of 3-200 µM, and for Gd-TPMTA the

19   range was 25-200 µM; concentrations lower than 25 µM were not tested because of sensitivity

1   limits owing to the broader EPR spectrum of Gd-TPMTA. A few examples of echo-decay data and

2   their fits are shown in **Fig. S8.** The concentration dependence of $1/T_m$ measured at 10 K on the CT

3   for the PyMTA variants is given in **Fig. 4*A***. We chose 10 K because it is the optimal temperature

4   for DEER measurements considering the populations of the CT and the T_m temperature

5   dependence (Goldfarb, 2014). We did not detect any apparent effect of the degree of deuteration

6   on T_m and β, both of which show a clear concentration dependence. This indicates that protons

7   with hyperfine couplings in the range of 1-2 MHz (distance < 5 Å) do not lead to decoherence as

8   they may be within the nuclear spin diffusion barrier(Wolfe, 1973).

9   $1/T_m$ of Gd-PyMTA is linearly dependent on concentration, [C], and the intercept of 0.05 μs^{-1} gives

10 $T_m(0)$=20 μs, this is T_m free of SD contributions. The dependence of β on [C] is not linear, reaching

11 β=1 for [C]$\rightarrow$0 (**Fig. 4B**). The dependence of $1/T_m$ on the magnetic field within the EPR spectrum

12 (10 K and [C]=200 μM), shown in **Fig. 4C**, reveals the same dependence as reported

13 earlier(Raitsimring et al., 2014), where the central transition exhibits a longer T_m, a characteristic

14 of the tZFS mechanism (Raitsimring et al., 2014). The Hahn echo decay behavior of Gd-TPMTA,

15 presented in **Fig. 4D-F,** was generally like that of Gd-PyMTA, disclosing no dependence on the

16 deuteration levels. For Gd-TPMTA, the concentration dependence measurements were carried

17 out at three field positions (1,2,3, see **Fig. 2A**) within the CT, and the results of all three were

18 practically the same; the data presented in **Fig. 4 D-F** corresponds to position 1. For Gd-TPMTA

19 $T_m(0)$=10 μs, the value of β is lower than for Gd-PyMTA and β=0.8 for [C]$\rightarrow$0. In general, β in the

20 range of 1-2.5 suggests the presence of a fast dephasing process attributed to SD or NSD(Salikhov

21 et al., 1981; Eaton and Eaton, 2000), whereas β<1 is typical of slow processes or is a signature of

22 relaxation time distribution(Salikhov et al., 1981). Accordingly, we attribute the reduction in β

23 with concentration to a reduction in the SD contribution, and the lower value of β at the low

24 concentration limit of Gd-TPMTA is likely due to a larger, more extensive distribution of relaxation

25 times. The latter arises from the larger ZFS and the significant contributions of transitions other

26 than the CT at the CT field. We checked for the effect of ID for Gd-PyMTA with [C]= 200 μM by

27 measuring the echo decay as a function of the length of the second pulse and found a negligibly

28 small contribution to $1/T_m$ and β (see **Fig. S9**). Therefore, we conclude that the contribution of ID

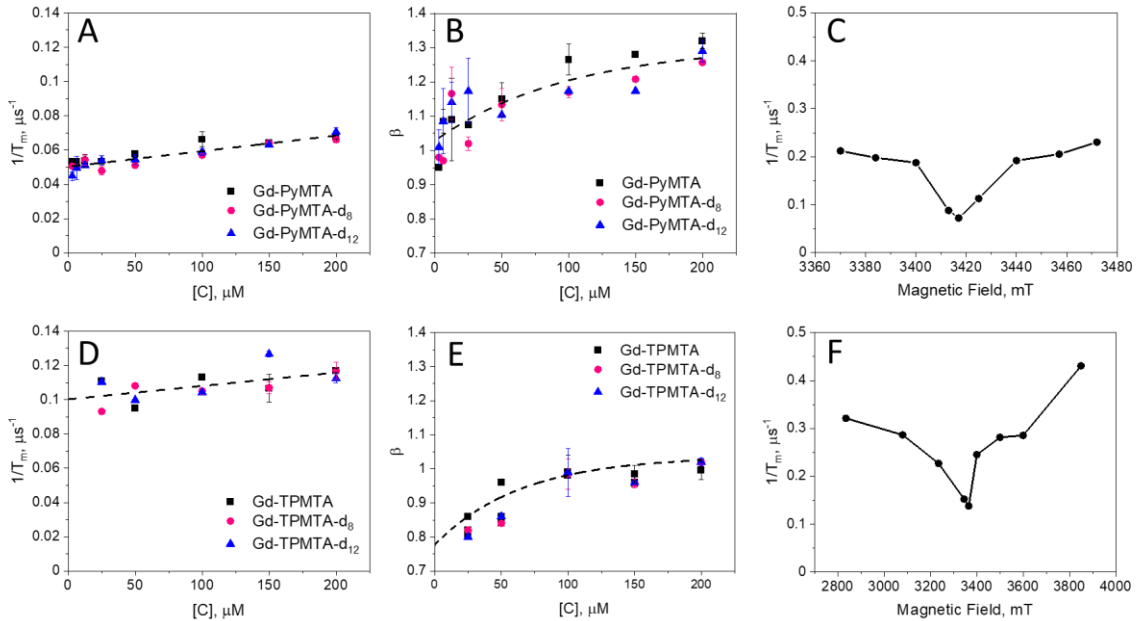29 to the concentration dependence of $1/T_m$ is minimal.

Figure 4. The dependence of $1/T_m$ and β, measured at 10 K and the peak of the CT for the Gd-PyMTA variants (A,B) and Gd-TPMTA variants (D,E) measured at position 1 given in Fig. 2A and 2B, respectively. The dotted line in A and D is the linear fit with slopes of $9.07 \times 10^{-5} \pm 8.2 \times 10^{-6}$ and $7.79 \times 10^{-5} \pm 2.9 \times 10^{-5}$ $(\mu s \cdot \mu M)^{-1}$ and intercepts of 0.05 ± 0.01 and 0.100 ± 0.003 μs^{-1} for Gd-PyMTA and Gd-TPMTA, respectively. The dotted lines in B and E were obtained with an exponential function $y = y_0 + A_1 e^{-\left(\frac{x}{T}\right)}$ to guide the eye. The parameters used were $y_0=1.3$, A=-0.28, T=100.8 µM and $y_0=1.04$, A=-0.26, T=64.5 µM for Gd-PyMTA and Gd-TPMTA, respectively. (C, F) The Field dependence of $1/T_m$ for 200 µM Gd-PyMTA (C) and 200 µM Gd-TPMTA (D), measured at 10 K.

Because the T_1 values of Gd(III) are relatively short and can influence its phase relaxation, we carried out T_1 and T_m measurements at different temperatures for Gd-PyMTA and Gd-TPMTA. We measured only the non-deuterated variants as we did not see any effect of the complex deuteration on the echo decays. The T_1 values were determined from inversion recovery experiments and were analyzed using stretched exponents with values in the range of 0.7-0.8 (see **Fig. S10**). **Fig. 5A** shows the temperature dependence of T_1 and T_m of 200 and 50 µM Gd-PyMTA; as expected T_1 is concentration independent. For Gd-TPMTA a broader range of temperatures was accessed (1.6-15 K vs 10-20 K) and the results are given in **Fig. 5B**. For both complexes, we found that, unlike T_m, T_1 was independent of the field position within the EPR spectrum (**Fig. S11**); namely, it is the same for all Gd(III) EPR transitions. For Gd(III), we must consider that it is not only the relaxation times that change with temperature but also the relative populations of the various transitions. Accordingly, changes in the levels' populations can influence the T_m values measured

1   at the CT. This effect is marginal for the temperature range explored for Gd-PyMTA but can be

2   significant for Gd-TPMTA below 7K.

3   To reveal the effect of T_1 on T_m, we plotted $1/T_m$ *vs* $1/T_1$, and the results are shown in **Figs. 5C-D**.

4   We observed a linear correlation for Gd-PyMTA (50 μM and 200 μM). For Gd-TPMTA, where a

5   wider range of temperatures was probed, a linear correlation was observed only for the 5-15 K

6   range; below 5 K $1/T_m$ is fairly constant, indicating that the contribution of T_1 to the phase

7   relaxation is no longer significant.

8
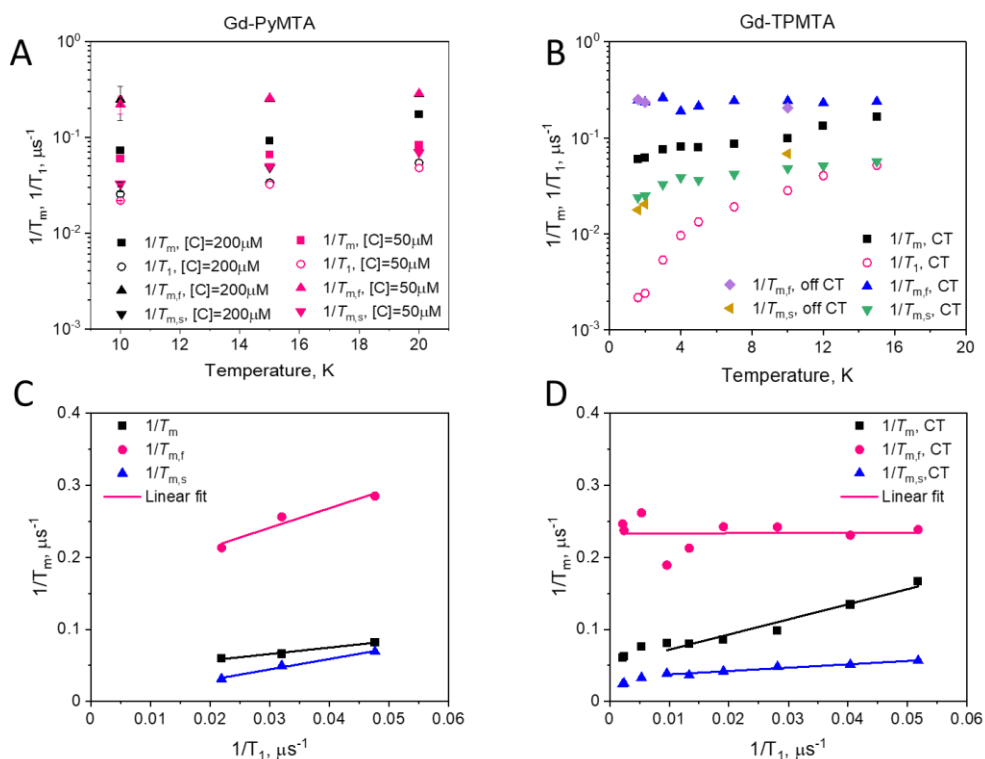
9   *Figure 5. The temperature dependence of $1/T_m$, determined with Hahn echo and CP trains, and*
10 *$1/T_1$ for Gd-PyMTA (A) and Gd-TPMTA (B). The dependence of $1/T_m$, determined with Hahn echo*
11 *and CP trains on $1/T_1$ for Gd-PyMTA (C) and Gd-TPMTA (D) along with the linear fit in the 6-20 K*
12 *range.*

13

14 The slopes of $1/T_m$ vs concentrations [C] for both complexes are the same within experimental

15 error **(Fig. 4)**. This indicates that the contribution of $1/T_{SD,ee}$ is negligible; otherwise a significant

16 difference would be expected because of the much broader EPR spectrum of Gd-TPMTA.

17 Therefore, we attribute the concentration dependence of $1/T_m$ to the indirect-T_1, $T_{SD,T1}$

18 mechanism, which is lineshape independent. As the two complexes have similar T_1 values, similar

1   slopes are expected. We used the known expressions for $T_{SD,T1,}$ and T_{ID} to estimate their theoretical

2   contributions (See **Fig. S12** and the associated text) for Gd-PyMTA. We found the predicted

3   contribution of T_{ID} is negligible, consistent with our experimental results, and that the $T_{SD,T1}$

4   calculated without any fitting parameters reproduces the experimental data reasonably (see **Fig.**

5   **S12**), predicting a slope in the linear region of 1.2×10^{-4} $\mu s^{-1}/\mu M$, compared to the experimental

6   slope 0.9×10^{-4} $\mu s^{-1}/\mu M$. The overestimated concentration dependence can result from the non-

7   exponential behavior of the echo decay and the inversion recovery, namely $\beta \neq 1$, and the

8   underestimation of T_1 determined by the inversion recovery sequence. The contributions to $T_m(0)$

9   can be from the direct-T_1 relaxation, $T_{m,T1}$, residual NSD, and tZFS. As the contributions of spin

10   diffusion, being either NSD or SD, to phase relaxation can be suppressed (refocused) by DD, we

11   proceeded with measurements of T_m using CP trains to further resolve the various contributions

12   to phase relaxation.

13   *3.1.3 CP with n≤5*

14   To resolve the potential contribution of NSD induced by the very weakly coupled protons on the

15   tags to decoherence, we followed the approach used by Jeschke and coworkers(Soetbeer et al.,

16   2018), and measured the intensity of the last echo as a function of the interval between the pulses

17   for CP trains with n=2-5 refocusing pulses (see **Fig. 6**), while holding the time between the first

18    $\pi/2$ pulse and the last echo equal to 2τ for all n. Interferences from overlapping stimulated echoes

19   can be eliminated by phase cycling up to n=5; beyond this, the phase cycle becomes too

20   demanding(Soetbeer et al., 2018) (the phase cycles used are listed in **Table S2**). The resulting echo

21   decays were analyzed using Eq.1 (examples of fits are shown in **Fig. S13**), and the data from the

22   protonated spin labels are given in **Fig. 7A**, where we plotted $1/T_m$ and β as a function of n, with

23   n=1 corresponding to the Hahn echo. We observed the same general behavior for 200 and 25 μM

24   Gd-PyMTA; an initial significant decrease in $1/T_m$ from n=1 to n=2, followed by a mild change

25   between n=2 to n=4 and leveling off at n=5. β exhibits a monotonic decrease from n=1 to n=3 and

26   levels off at n≥3, where it reaches a value of 1-1.2. Nevertheless, the systematically larger $1/T_m$

27   for 200 μM than that for 25 μM and the reduction of the differences between with n, shows that

28   DD can suppress SD for the 200 μM sample, though for n=5 only partially. The behavior of Gd-

29   TPMTA was similar, but less pronounced; $1/T_m$ decreases from n=1 to n=2 but then levels off and

30   β levels off between n=3 and n=4 and reached 0.9. We find the suppression of NSD contributions

31   to be less likely because Gd-TPMTA has more weakly coupled protons on the label, and therefore,

1   the effect should have been larger for Gd-TPMTA, but the opposite was observed. Such

2   measurements, reported for Gd-DOTA-M in D_2O:glycerol-d_8 (25 µM) at 10 K at Q-band, showed a

3   similar behavior, i. e. a mild decrease in $1/T_m$ and β (Soetbeer et al., 2021b). T_m reached 40 µs for

4   n=5 for Gd-DOTA-M, compared to 29 µs for Gd-PyMTA at W-band.
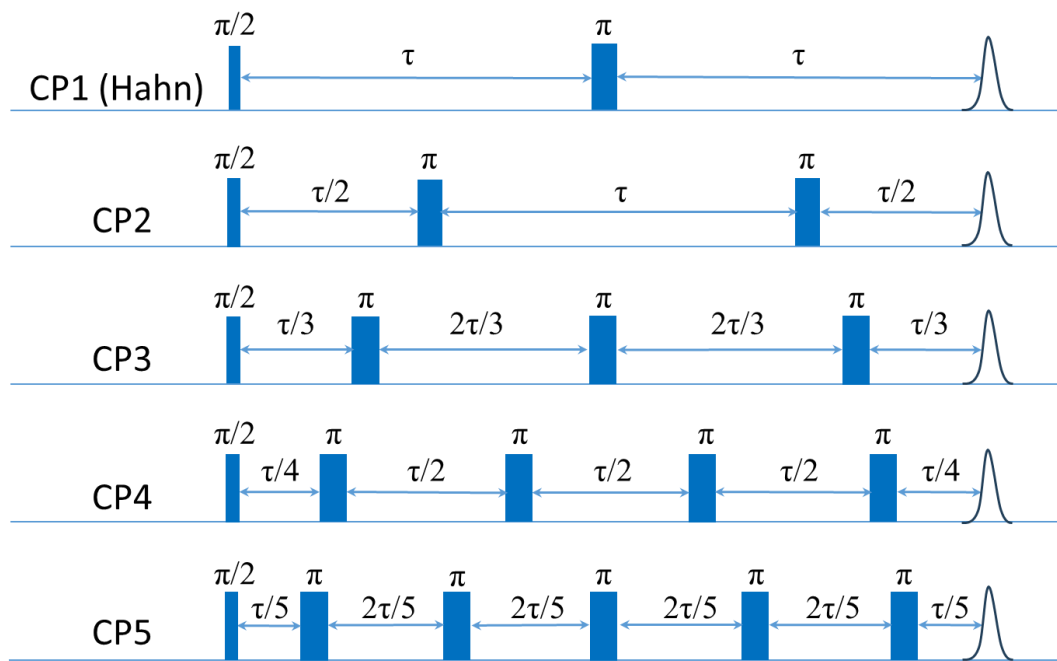
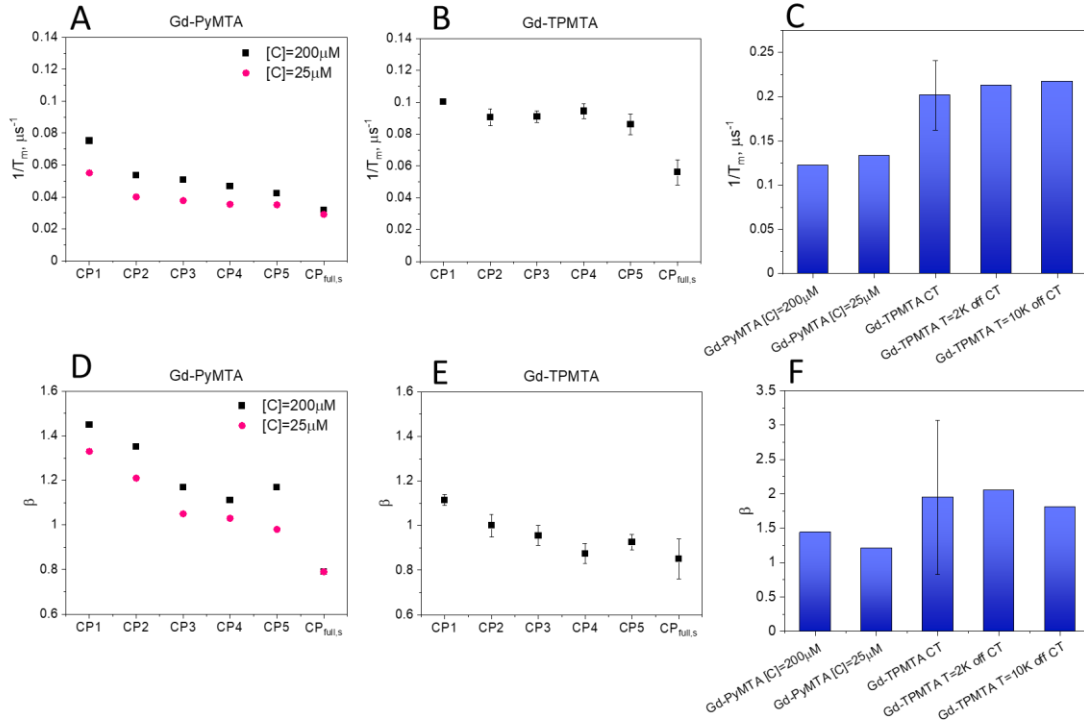6   *Figure 6. The CP sequences for n=1-5. n=1 corresponds to the Hahn echo.*

Figure 7. *Comparison of $1/T_m$ measured at the CT and 10 K (A,B) and β (D,E), determined by CP with n=1-5 and those of the slow component in the full CP train for Gd-PyMTA (A,D) and Gd-TPMTA (B,E). (C,F) Comparison of $1/T_m$ of the fast component in the full CP train (C) and β (F) for different complexes with different concentrations for Gd-PyMTA and Gd-TPMTA ([C]=200 μM) measured at different field positions within the EPR spectrum.*

3.1.4 Full CP train

The very mild effect of CPn with *n*=5 on the phase relaxation of both complexes prompted us to improve the effectiveness of the DD by applying a CP train pulse sequence with a constant inter-pulse delay τ (see **Fig. 8A**) and the shortest available on our spectrometer (290 ns), to suppress potential contributions from fast processes to the phase relaxation. We refer to this as full CP train. An example of the echo train produced by this sequence is given **Fig. 8B,** and the plot of the echo intensities as a function of time is presented in **Fig. 8C.** In this case, the data could not be satisfactorily fitted with a single stretched exponent and a sum of two stretched exponents (termed earlier as SSE (Soetbeer et al., 2018)) was used as follows:

$$y = A * exp\left(-\frac{t}{T_{m,f}}\right)^{\beta_f} + (1 - A) * exp\left(-\frac{t}{T_{m,s}}\right)^{\beta_s} \tag{2}$$

18

where t is the time between the first $\pi/2$ pulse and the observed echo, and the subscripts f and s correspond to fast and slow processes.

As mentioned earlier, CP measurements with pulses that are not ideal (selective) because of their small bandwidth compared to the EPR spectral width produce echoes that are not pure refocused echoes but have contributions from stimulated echoes that decay with some combination of T_1 and spectral diffusion (Kurshev and Raitsimring, 1990; Mitrikas, 2023). To ensure that the observed SSE analysis is not a consequence of the contributions of such unwanted echoes, we performed a series of calculations presented in the SI (**Figs. S14-S16**). These show that the stimulated echo contribution leads to overestimation of T_m by no more than 20% and that a single stretched exponential function can fit the calculated echo intensities. To further ensure that the two observed components derived from the experimental results are not a consequence of artifacts in the applied pulse sequence, we carried out similar measurements on a nitroxide (MTSL) spin label in D_2O:glycerol-d_8 (25 μM), and the results are shown in **Fig. S17**. In this case, the echo train could be fitted well with only one stretched exponent. Therefore, we concluded that the two resolved populations are intrinsic to the Gd(III) complexes studied and are not a consequence of the stimulated echo contributions or experimental artifacts.
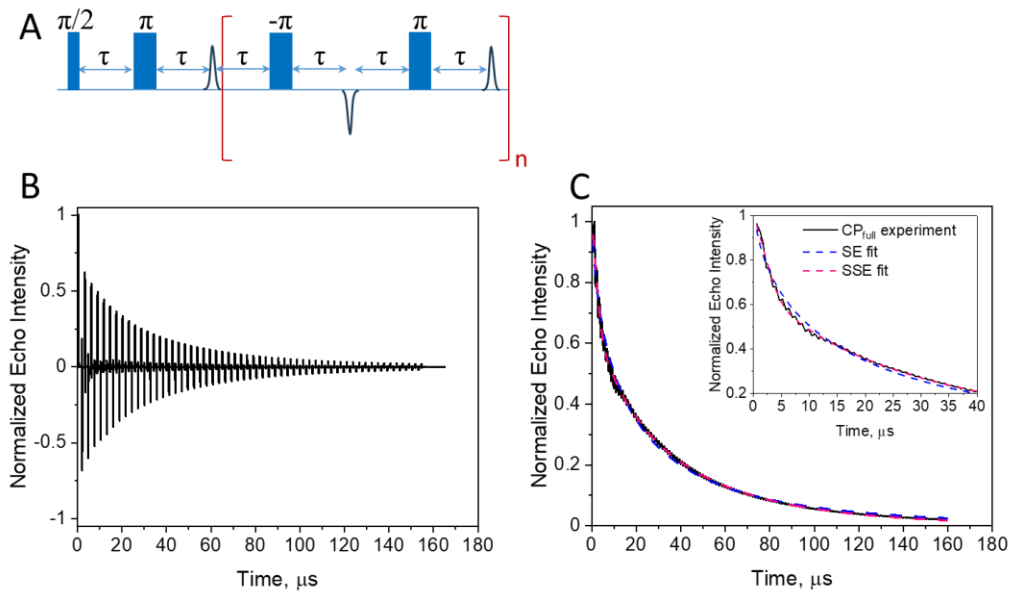

Figure 8. (A) The full CP train sequence (n=137, τ=290 ns) applied and (B) the resulting echo train for Gd-PyMTA, 50 μM, measured at 10 K and the maximum of the CT. (C) The plot of the integrated echo intensity of the individual echoes as a function of time, with the data fit using a single stretched exponential and a sum of two stretched exponentials. The inset shows an expanded part of the trace, highlighting the fit differences. The fitting parameters were: T_m=32 μs, β=0.58, A=1.1

1 *for SE fit (eq. 1) and $T_{m,f}$=3.3 µs, β_f=1.85, A=0.25, $T_{m,s}$=29.6 µs, β_s=0.78 (eq.2) for SSE fit,*
2 *respectively.*

3

4 **Fig. 9** summarizes the dependence of the slow and fast CP decay rates, $1/T_{m,s}$ and $1/T_{m,f}$, and the

5 associated β_s and β_f, on concentration and temperature for all Gd-PyMTA and Gd-TPMTA variants.

6 The slow component of Gd-PyMTA, which has a contribution of 75-80%, is concentration and

7 deuteration independent, and at 10 K T_m is 35 µs, about twice as long as that measured by the

8 Hahn echo decay (18 µs), well beyond the 20% expected overestimation due to the selectivity of

9 the applied pulses. The same holds for β, which is reduced to about 0.75. For comparison with the

10 values obtained with CP1-CP5 we added the data to **Fig. 7A,D.** Interestingly, while CP5 could not

11 eliminate the concentration dependence, the entire train did (n~140). Here, the $1/T_{m,s}$ values for

12 25 and 200 µM Gd-PyMTA coincided. We should bear in mind that the full CP train and CP*2-CP5*

13 are different types of experiments; for the former, the number of π pulses and τ are held constant

14 and the recorded signal is the intensity of the occurring refocused echo after each π pulse, and

15 for the latter the number of pulses is constant, τ is varied and the intensity of the last echo is

16 measured. The short τ used in the full CP train seemed to refocus the SD contributions better than

17 the CP5 experiment. We verified that by increasing τ in the full CP train the decay rate increased.

18 There is an increase in $1/T_{m,s}$ with temperature, whereas β_s and the relative population remain

19 constant. For Gd-TPMTA, as for Gd-PyMTA, the slow component is not dependent on

20 concentration nor deuteration level. Still, there is an increase of β_s and a decrease in its relative

21 population with increasing temperatures. The values of $1/T_{m,s}$ and β_s at 10 K are added to **Fig. 7B,E**

22 for comparison with those obtained for *CP1-CP5*. The dependence of $1/T_{m,s}$ on the temperature

23 and $1/T_1$ for the two complexes are shown in **Fig. 5.**

24 For the fast component, the spread of the data points is quite large for all variants, and no

25 systematic variation in concentration nor deuteration is observed. Here, $T_{m,f}$ is 3-6 µs and β_f=1.3-

26 3; no temperature or concentration dependence was detected within the experimental error. A

27 comparison of the various values of $1/T_{m,f}$, and β_f for different samples and temperatures is given

28 in **Fig. 7C,F.** The relative contribution of the two components is fairly constant in the temperature

29 range tested for Gd-PyMTA, whereas for Gd-TPMTA the contribution of the fast component is

30 constant for 1.6-4 K and thereafter, a significant increase with increasing temperature is observed

1   in the range of 6-15 K **(Fig. 10)**. This trend seems to correlate with the relative intensity of the

2   central transition (**Fig. 2**). Currently, we do not have an explanation for this behavior.
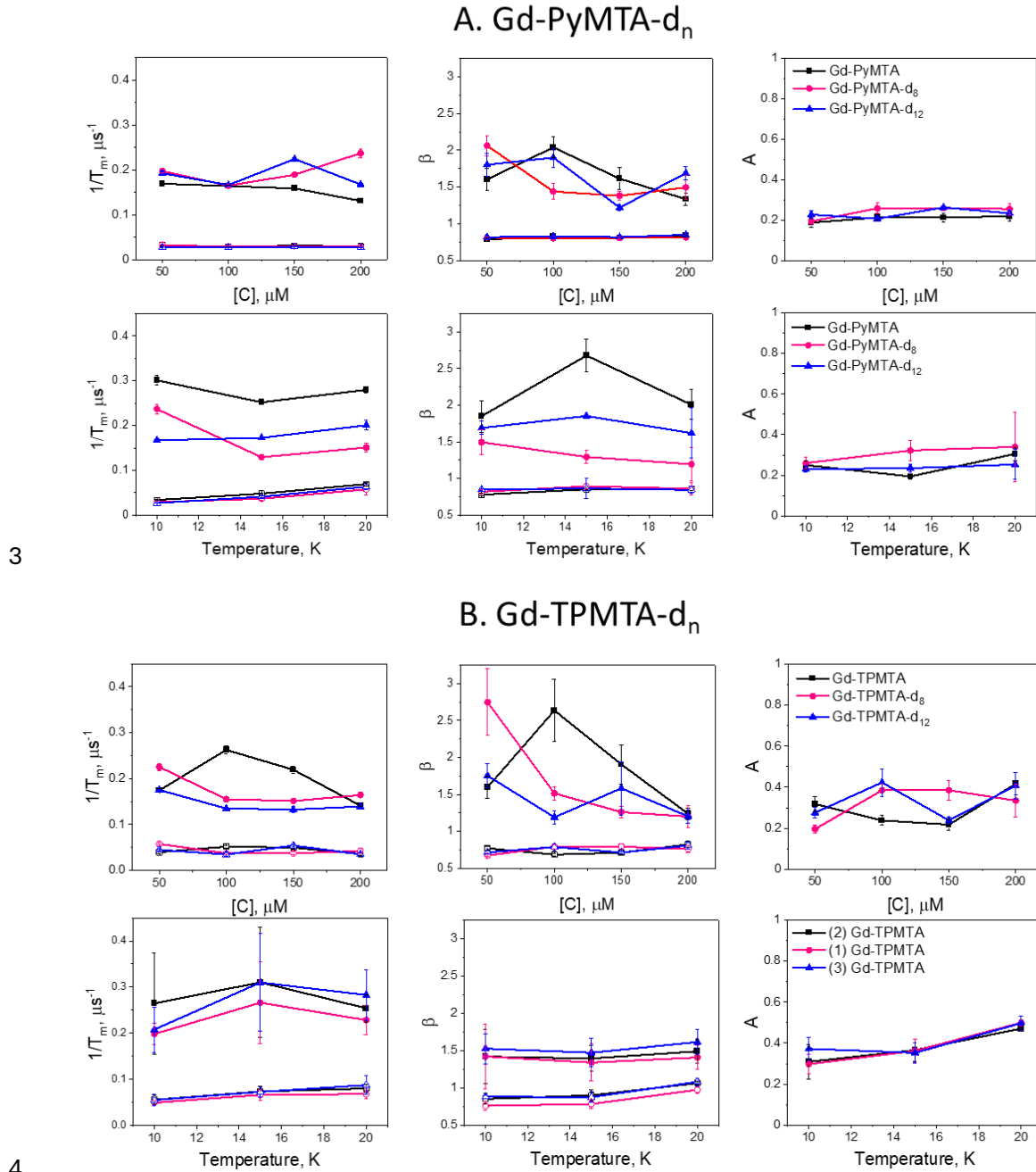
3

4

5   *Figure 9. The dependence of the slow (open symbols) and fast (filled symbols) CP full train decay*
6   *rates, the associated stretched exponent and their relative population measured for: (A) The Gd-*
7   *PyMTA samples measured at the peak of the central transition as a function of concentration (10*
8   *K) and as a function of temperature for 200 μM. (B) The Gd-TPMTA samples measured at position*
9   *1 in the central transition as a function of concentration (10 K) and as a function of temperature*
10   *for 200 μM Gd-TPMTA at field positions 1,2,3. The field positions are defined in* **Fig. 2.**

1
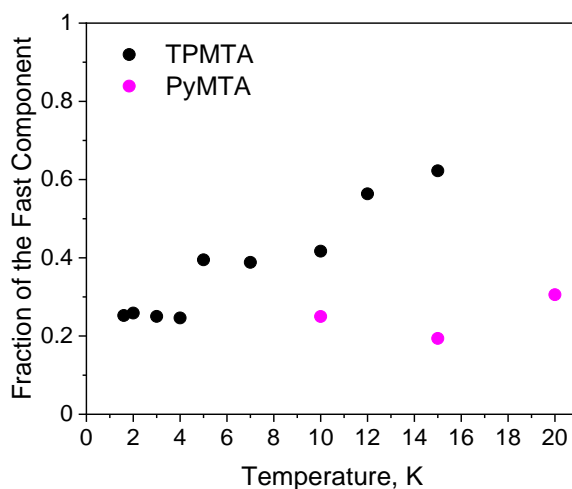
Figure 10. The dependence of the relative contribution of the fast component, measured at the CT (position 1), as a function of temperature for Gd-PyMTA (magenta, [C] = 200µM) and Gd-TPMTA (black, [C] = 200µM).

We also investigated the field dependence of the decay rates of two components at two temperatures, 10 and 20 K (**Fig. 11**). For the Hahn echo, we observed a clear enhancement of the decay rate outside the CT (see **Fig. 4 C,F**); in contrast, the slow component showed a minimal change across the CT at both temperatures. Also, the difference between the CT and the other transitions was significantly weaker for the fast component than for the Hahn echo. Interestingly, the contrast between the CT and the other transitions is manifested in the two components' relative contributions. For both complexes, the contribution of the fast component is lower at the CT than outside the CT, and the contribution of the fast component increases with temperature in all fields.
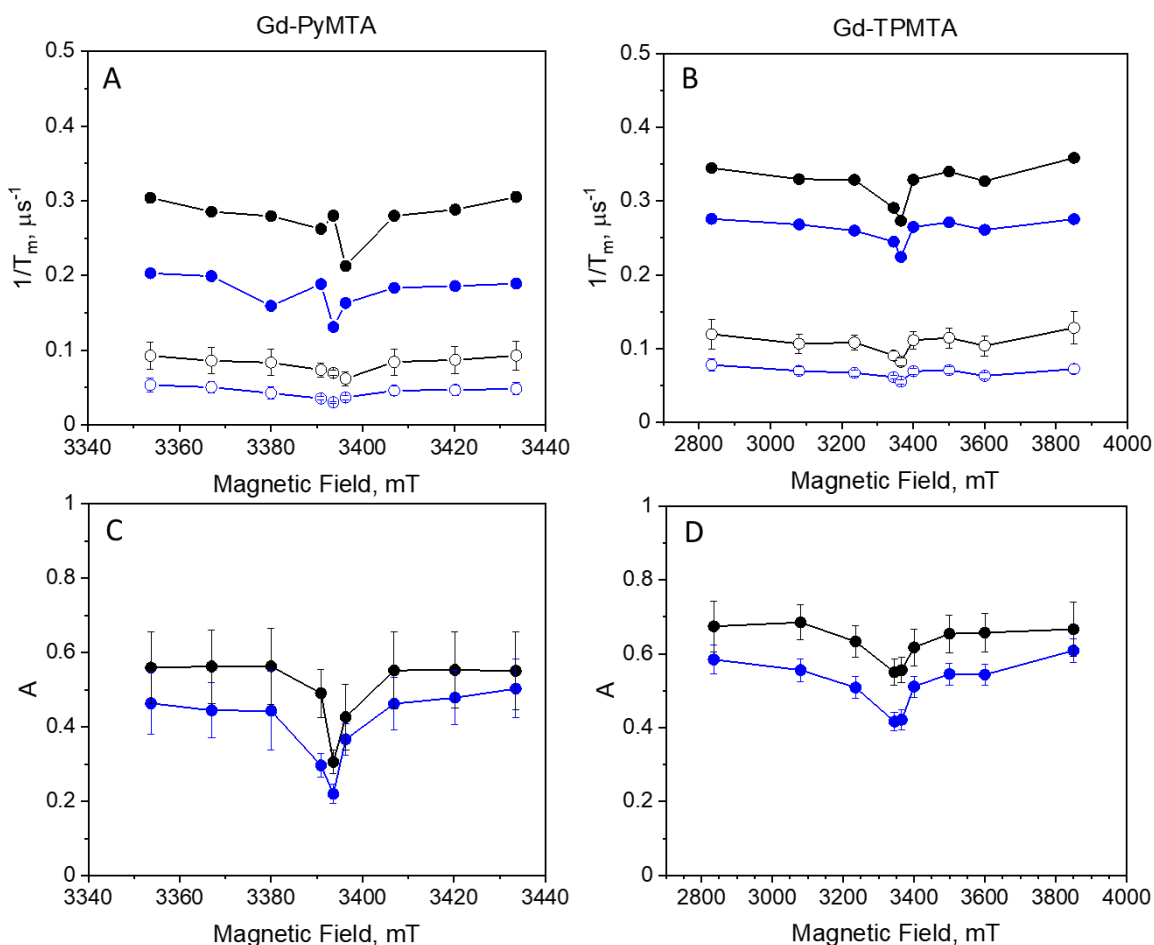
22

Figure 11. *A. The field dependence of $1/T_m$ for the slow (empty symbols) and fast (full symbols)*
3 *components at 10 (blue) and 20 K (black) of Gd-PyMTA ([C] = 200 μM) and B. Gd-TPMTA ([C] =*
4 *200 μM). C. The relative contribution of the fast component, A (see Eq. (2), for Gd-PyMTA and for*
5 *D. Gd-TPMTA.*

6

7   From the full CP train measurements, we conclude that (i) two populations of spins with different

8   dominating phase relaxation mechanisms are observed for the two complexes. (ii) Any residual

9   SD_{ee} and SD_{T1} contributions are suppressed under the CP train conditions. (iii) We tentatively

10   assign the dominating mechanism that governs the slow-relaxing population to the direct-T_1

11   mechanism and tZFS for the fast-relaxing population. (iv) The relative contribution of the tZFS

12   mechanism is lower at the central transition than at the other transitions. (v) Gd-TPMTA, which

13   has a significantly larger ZFS than Gd-PyMTA, has a larger population dominated by the tZFS,

1   which is also temperature-dependent. The temperature dependence seems to follow the relative

2   intensity of the CT with temperature.

3   <u>3.2. Influence of protein deuteration.</u>

4   For nitroxide spin labels, protein deuteration increases T_m by a factor of ~4 (Ward et al., 2010;

5   Schmidt et al., 2016). To see if Gd(III) spin labels experience the same effect, after exploring the

6   phase relaxation behavior of the free Gd-PyMTA and Gd-TPMTA spin labels in deuterated

7   solvents, we proceeded to examine their phase relaxation after their attachment to protonated

8   and deuterated proteins in deuterated solvents. Ubiquitin D39C/E64C was labeled with Gd-

9   PyMTA and Gd-TPMTA, producing doubly labeled proteins typically used for DEER applications.

10   The concentrations were ~25 μM and ~50 μM for Gd-PyMTA and Gd-TPMTA labeled ubiquitin,

11   respectively. The Hahn echo decays were fitted using Eq.1, as was done for the free labels

12   (examples are shown in **Fig. S18**), and the results are summarized in **Fig. 12** for measurements on

13   the CT at 10 K. The attachment to [1]H-ubiquitin increased $1/T_m$ by a factor of 2.4 for Gd-PyMTA

14   and 1.8-1.9 for Gd-TPMTA, with no significant effect on the degree of label deuteration. While

15   protein deuteration led to a slight decrease of $1/T_m$ (~10%) for Gd-PyMTA, for Gd-TPMTA labeled

16   ubiquitin a significant effect was noticed only for Gd-TPMTA-d_{12}, almost reaching the value of the

17   free label. The dependence of β on protein deuteration is insignificant for Gd-TPMTA. In contrast,

18   for Gd-PyMTA, a gradual decrease with the increased degree of the label deuteration is observed

19   for the deuterated protein, where for Gd-PyMTA-d_{12} it reaches $\beta=1$, as for the free label. A small

20   effect of the protein deuteration was also observed for the Gd-DO3A labeled ubiquitin (50 μM)

21   (**Fig. 12**). The low impact of protein deuteration on the Gd(III) T_m values compared to nitroxide

22   can be attributed to the Gd(III)'s much shorter T_1, which provides the upper limit to T_m ($T_m \leq 2T_1$).

23   A comparison of the T_m and β values measured by Hahn echo decay for the free labels and the

24   protein samples is given in Table S3.

25   To further explore the origin of the significant reduction in the phase relaxation rate while bound

26   to protein and the small effect of protein deuteration, we carried out full CP train measurements

27   on the protonated and deuterated protein samples for Gd-PyMTA and Gd-TPMTA. Like the free

28   labels, the data could not be fitted well with one stretched exponent, and a sum of two such

29   exponents was needed, one with a fast decay and the other with a slow decay **(see Fig. S19).** The

30   results for the population with the slow decay for protonated and deuterated ubiquitin with

31   protonated Gd-PyMTA are shown in **Fig. 12**. The difference between the protonated and

deuterated proteins was small. Same as in the case of the free label, we observed a reduction of about a factor of 2 in $1/T_m$ for the slow population under CP train conditions, as compared to the value for Hahn echo. Interestingly, $1/T_m$ in the free Gd-PyMTA in a deuterated solvent is smaller by a factor of about two compared to the protein value. The same behavior was observed for Gd-TPMTA.

What is the source of the faster phase relaxation in the protein compared to the free complex? It cannot be attributed to the direct-T_1 mechanism because of the similar T_1 values, 50.5 μs for protein and 45.5 μs for free complex. One possibility could be NSD from the non-deuterated HEPES molecules used as buffer, which results in 2.5% protons in the solvent. Another possibility could be the lower amount of glycerol in the protein samples (8:2 v/v vs 1:1 v/v for free Gd-PyMTA). To check this possibility, we prepared solutions of Gd-PyMTA in 15 mM HEPES in 8:2 v/v vs 1:1 v/v D_2O/glycerol-d_8 and measured their Hahn-echo decays at 10 K. The results, given in **Fig. S20**, show that the contribution of the protonated HEPES is small, but that of the lower amount of glycerol is significant because of enhanced instantaneous diffusion due to a poorer quality of the glass leading to higher local concentrations. These two effects account only for about 80% of shorter T_m in the protein. An additional contribution can come from the fact that the proteins are doubly labeled, i.e., every Gd(III) center has a neighbor ~4.2 nm away from it (see **Fig. S21**). Accordingly, its phase relaxation can be affected by indirect T_1 due to the neighbor, which is concentration-independent. The relaxation of this neighbor is responsible for the Gd(III)-Gd(III) RIDME (Relaxation-Induced Dipolar Modulation Enhancement) PD-EPR experiment, where it undergoes both single, double and triple quantum flips during the mixing time.(Razzaghi et al., 2014). In this case, mutual Gd(III) pair flip-flops can also induce relaxation.(Tyryshkin et al., 2012)
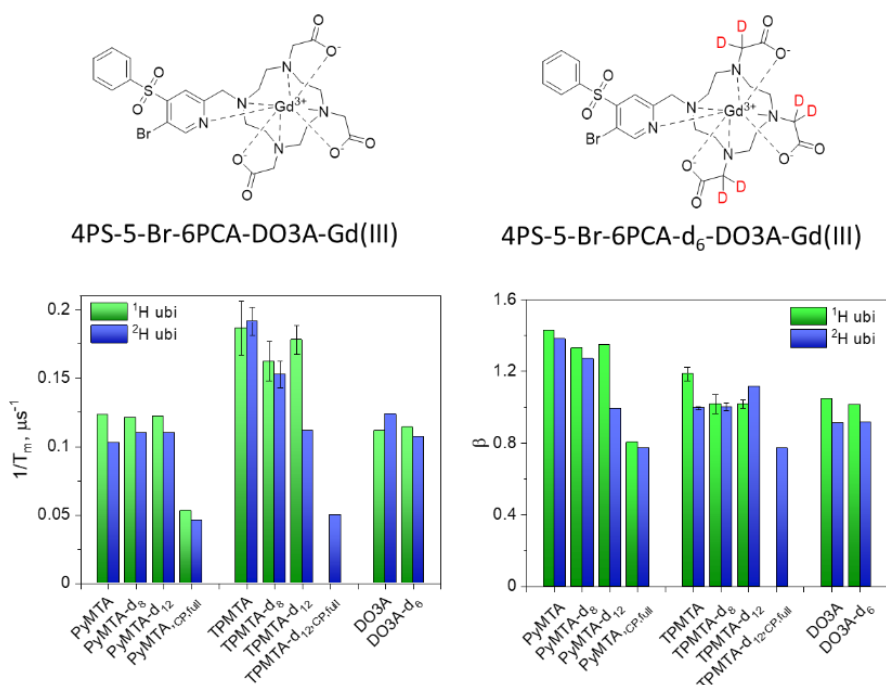
1

6 **Conclusions.**

7 In this work, we explored the mechanisms responsible for the phase relaxation of Gd(III) spin

8 labels at 95 GHz, exploring whether deuteration of the label or the protein can extend the phase

9 relaxation. To resolve the relaxation mechanisms, we first studied the free label with different

10 degrees of deuterations in a deuterated solvent and examined both concentration and

11 temperature dependencies. We compared two labels having very different ZFSs, which helped

12 resolve various relaxation mechanisms. T_m was determined from both Hahn echo decay and CP

13 echo trains. Our conclusions are as follows:

14   1. Protons with hyperfine couplings in the 1-2 MHz range, situated at distances <5 Å from

15   the gadolinium ion, do not affect T_m and are located within the nuclear spin diffusion

16   barrier.

17   2. In the range of 5-200 μM the concentration dependence of the free tag is primarily

18   determined by the indirect T_1- induced mechanism.

3. At the limit of [C]→0, the contributions to T_m (0) can be residual NSD of the protons on the pyridine and phenyl rings with hyperfine couplings below 0.4 MHz or residual protons in the deuterated matrix, tZFS, and direct T_1. Since $T_m(0)$ for Gd-TPMTA is shorter by a factor of about 2 and T_1 values of both complexes are similar, we attribute the difference to the increased contribution of residual NSD and tZFS. Gd-TPMTA has 12 weakly coupled protons vs 7 for Gd-PyMTA, and its ZFS is significantly larger. In principle, it would be possible to predict the contribution of the above-mentioned weakly coupled protons and residual solvent protons to the Hahn echo decay using the analytical pair product approximation, which allows for computationally efficient simulations and provides a good prediction (Canarie et al., 2020; Jeschke, 2023). This, however, is beyond the scope of this manuscript.

4. The CPn measurements with n=2-5 had a more substantial suppression effect on T_m for Gd-PyMTA than on Gd-TPMTA, suggesting that it has contributions from SD due to electron-electron interactions and that NSD was not suppressed under these conditions (n=5).

5. Full CP train measurements (n~140) resolved the presence of two populations: one with a slow phase relaxation and the other with a fast one. The dominating mechanism for the slow population is direct-T_1. Its T_m showed no concentration dependence and was longer by a factor of about 2 relative to the Hahn echo decay for both complexes, yet keeping their relative values. We tentatively assign the decrease in $1/T_{m,s}$ to full suppression of the residual indirect T_1-induced and NSD mechanism, made possible by the relatively short τ=290 ns used in the full train. This is supported by the more significant difference between n=5 and the full CP train for Gd-TPMTA, which has more distant protons.

6. For the fast relaxing population, $1/T_{m,f}$ is larger for Gd-TPMTA; therefore, we assign it to populations where the tZFS dominates, supported by its more extensive field dependence than $1/T_{m,s}$.

7. Because of the relatively short T_1 and the contribution of the tZFS mechanism, protein deuteration does not significantly affect T_m. The shorter T_m for the doubly labeled proteins is attributed primarily to the lower glycerol amount in the sample and indirect- T_1 owing to the presence of a close-by Gd(III) neighbor.

The above shows that prolonging T_m would require increasing T_1, which can be achieved by lowering the temperature. However, this will be at the expense of the CT population, thus

reducing sensitivity in DEER measurements. Another option is to reduce the spectrometer frequency, which will cause broadening of the CT and impede sensitivity. Yet another way to increase T_m is to choose a label with a smaller ZFS (Ossadnik et al., 2025). A very small ZFS, however, introduces significant difficulties in analyzing DEER data for distances below 3 nm unless the excitation of the CT is avoided (Dalaloyan et al., 2015).

Author contribution: EE-investigation, visualization, writing – review and editing. XZ-investigation, visualization CC-investigation. YY-investigation. AB-formal analysis, methodology, writing – review and editing. GM -formal analysis, visualization, writing – review and editing XS-Conceptualization, funding acquisition, supervision, writing – review and editing.   DG - Conceptualization, funding acquisition, supervision, writing – original draft preparation.

Competing interests : DG is a member of the executive editorial board of Magnetic Resonance.

Acknowledgments.

References

Canarie, E. R., Jahn, S. M., and Stoll, S.: Quantitative Structure-Based Prediction of Electron Spin Decoherence in Organic Radicals, J. Phys. Chem. Lett., 11, 3396-3400, 10.1021/acs.jpclett.0c00768, 2020.

Dalaloyan, A., Qi, M., Ruthstein, S., Vega, S., Godt, A., Feintuch, A., and Goldfarb, D.: Gd(III)-Gd(III) EPR distance measurements--the range of accessible distances and the impact of zero field splitting, Phys. Chem. Chem. Phys., 17, 18464-18476, 10.1039/c5cp02602d, 2015.

Eaton, S. S. and Eaton, G. R.: Relaxation Times of Organic Radicals and Transition Metal Ions, in: Distance Measurements in Biological Systems by EPR, edited by: Berliner, L. J., Eaton, G. R., and Eaton, S. S., Springer US, Boston, MA, 29-154, 10.1007/0-306-47109-4_2, 2000.

Epel, B., Arieli, D., Baute, D., and Goldfarb, D.: Improving W-band pulsed ENDOR sensitivity-random acquisition and pulsed special TRIPLE, J. Magn. Reson., 164, 78-83, 10.1016/s1090-7807(03)00191-5, 2003.

1 Feintuch, A., Shimon, D., Hovav, Y., Banerjee, D., Kaminker, I., Lipkin, Y., Zibzener, K., Epel, B.,
2 Vega, S., and Goldfarb, D.: A Dynamic Nuclear Polarization spectrometer at 95 GHz/144 MHz
3 with EPR and NMR excitation and detection capabilities, J. Magn. Reson., 209, 136-141,
4 10.1016/j.jmr.2010.12.010, 2011.

5 Garbuio, L., Zimmermann, K., Häussinger, D., and Yulikov, M.: Gd(III) complexes for electron–
6 electron dipolar spectroscopy: Effects of deuteration, pH and zero field splitting, J. Magn.
7 Reson., 259, 163-173, https://doi.org/10.1016/j.jmr.2015.08.009, 2015.

8 Giannoulis, A., Ben-Ishay, Y., and Goldfarb, D.: Characteristics of Gd(III) spin labels for the study
9 of protein conformations, Meth. Enzymol., 651, 235-290, 10.1016/bs.mie.2021.01.040, 2021.

10 Goldfarb, D.: Gd3+ spin labeling for distance measurements by pulse EPR spectroscopy,
11 Phys.Chem.Chem.Phys., 16, 9685-9699, 10.1039/C3CP53822B, 2014.

12 Gromov, I., Krymov, V., Manikandan, P., Arieli, D., and Goldfarb, D.: A W-band pulsed ENDOR
13 spectrometer: Setup and application to transition metal centers, J. Magn. Reson., 139, 8-17,
14 10.1006/jmre.1999.1762, 1999.

15 Hansen, S. H., Buch, C. D., Petersen, J. B., Rix, M., Ubach I Cervera, M., Strandfelt, A., Winpenny,
16 R. E. P., McInnes, E. J. L., and Piligkos, S.: Probing decoherence in molecular 4f qubits, Chem. Sci.,
17 15, 20328-20337, 10.1039/D4SC05304D, 2024.

18 Jeschke, G.: Nuclear pair electron spin echo envelope modulation, Journal of Magnetic
19 Resonance Open, 14-15, 100094, https://doi.org/10.1016/j.jmro.2023.100094, 2023.

20 Kurshev, V. V. and Raitsimring, A. M.: Carr-Purcell train in the conditions of partial excitation of
21 magnetic resonance spectrum, J. Magn. Reson. (1969), 88, 126-129,
22 https://doi.org/10.1016/0022-2364(90)90113-N, 1990.

23 Li, J. and Byrd, R. A.: A simple protocol for the production of highly deuterated proteins for
24 biophysical studies, J. Biol. Chem., 298, 102253, https://doi.org/10.1016/j.jbc.2022.102253,
25 2022.

26 Mentink-Vigier, F., Collauto, A., Feintuch, A., Kaminker, I., Le, V. T., and Goldfarb, D.: Increasing
27 sensitivity of pulse EPR experiments using echo train detection schemes, J. Magn. Reson., 236,
28 117-125, 10.1016/j.jmr.2013.08.012, 2013.

29 Mitrikas, G.: Long Electron Spin Coherence Times of Atomic Hydrogen Trapped in Silsesquioxane
30 Cages, J. Phys. Chem. Lett., 14, 9590-9595, 10.1021/acs.jpclett.3c02626, 2023.

31 Mocanu, E. M., Ben-Ishay, Y., Topping, L., Fisher, S. R., Hunter, R. I., Su, X.-C., Butler, S. J., Smith,
32 G. M., Goldfarb, D., and Lovett, J. E.: Robustness and Sensitivity of Gd(III)–Gd(III) Double
33 Electron–Electron Resonance (DEER) Measurements: Comparative Study of High-Frequency EPR
34 Spectrometer Designs and Spin Label Variants, Appl. Magn. Reson., 56, 591-611,
35 10.1007/s00723-024-01741-0, 2025.

36 Montgomery, J. R. D., Lancefield, C. S., Miles-Barrett, D. M., Ackermann, K., Bode, B. E.,
37 Westwood, N. J., and Lebl, T.: Fractionation and DOSY NMR as Analytical Tools: From Model
38 Polymers to a Technical Lignin, ACS Omega, 2, 8466-8474, 10.1021/acsomega.7b01287, 2017.

39 Ossadnik, D., Kuzin, S., Qi, M., Yulikov, M., and Godt, A.: A GdIII-Based Spin Label at the Limits
40 for Linewidth Reduction through Zero-Field Splitting Optimization, Inorganic Chemistry, 62, 408-
41 432, 10.1021/acs.inorgchem.2c03531, 2023.

Ossadnik, D., Qi, M., Voss, J., Keller, K., Yulikov, M., and Godt, A.: A Set of Three GdIII Spin Labels with Methanethiosulfonyl Groups for Bioconjugation Covering a Wide Range of EPR Line Widths, The Journal of Organic Chemistry, 90, 1847-1876, 10.1021/acs.joc.4c02441, 2025.

Pannier, M., Veit, S., Godt, A., Jeschke, G., and Spiess, H. W.: Dead-Time Free Measurement of Dipole–Dipole Interactions between Electron Spins, J. Magn. Reson., 142, 331-340, https://doi.org/10.1006/jmre.1999.1944, 2000.

Raitsimring, A., Dalaloyan, A., Collauto, A., Feintuch, A., Meade, T., and Goldfarb, D.: Zero field splitting fluctuations induced phase relaxation of Gd3+ in frozen solutions at cryogenic temperatures, J. Magn. Reson., 248, 71-80, https://doi.org/10.1016/j.jmr.2014.09.012, 2014.

Raitsimring, A., Astashkin, A. V., Enemark, J. H., Kaminker, I., Goldfarb, D., Walter, E. D., Song, Y., and Meade, T. J.: Optimization of Pulsed-DEER Measurements for Gd-Based Labels: Choice of Operational Frequencies, Pulse Durations and Positions, and Temperature, Appl. Magn. Reson., 44, 649-670, 10.1007/s00723-012-0434-6, 2013.

Raitsimring, A. M., Astashkin, A. V., Poluektov, O. G., and Caravan, P.: High-field pulsed EPR and ENDOR of Gd3+ complexes in glassy solutions, Appl. Magn. Reson., 28, 281-295, 10.1007/BF03166762, 2005.

Razzaghi, S., Qi, M., Nalepa, A. I., Godt, A., Jeschke, G., Savitsky, A., and Yulikov, M.: RIDME Spectroscopy with Gd(III) Centers, J. Phys. Chem. Lett., 5, 3970-3975, 10.1021/jz502129t, 2014.

Salikhov, K. M., Dzuba, S. A., and Raitsimring, A. M.: The theory of electron spin-echo signal decay resulting from dipole-dipole interactions between paramagnetic centers in solids, J. Magn. Reson. (1969), 42, 255-276, https://doi.org/10.1016/0022-2364(81)90216-X, 1981.

Schmidt, T., Wälti, M. A., Baber, J. L., Hustedt, E. J., and Clore, G. M.: Long Distance Measurements up to 160 Å in the GroEL Tetradecamer Using Q-Band DEER EPR Spectroscopy, Angew. Chem. Intl. Ed., 55, 15905-15909, https://doi.org/10.1002/anie.201609617, 2016.

Seal, M., Feintuch, A., and Goldfarb, D.: The effect of spin-lattice relaxation on DEER background decay, J. Magn. Reson., 345, 107327, https://doi.org/10.1016/j.jmr.2022.107327, 2022.

Soetbeer, J., Hülsmann, M., Godt, A., Polyhach, Y., and Jeschke, G.: Dynamical decoupling of nitroxides in o-terphenyl: a study of temperature, deuteration and concentration effects, Phys.Chem.Chem.Phys., 20, 1615-1628, 10.1039/C7CP07074H, 2018.

Soetbeer, J., Ibáñez, L. F., Berkson, Z., Polyhach, Y., and Jeschke, G.: Regularized dynamical decoupling noise spectroscopy – a decoherence descriptor for radicals in glassy matrices, Phys.Chem.Chem.Phys., 23, 21664-21676, 10.1039/D1CP03103A, 2021a.

Soetbeer, J., Millen, M., Zouboulis, K., Hülsmann, M., Godt, A., Polyhach, Y., and Jeschke, G.: Dynamical decoupling in water–glycerol glasses: a comparison of nitroxides, trityl radicals and gadolinium complexes, Phys.Chem.Chem.Phys., 23, 5352-5369, 10.1039/D1CP00055A, 2021b.

Stoll, S. and Schweiger, A.: EasySpin, a comprehensive software package for spectral simulation and analysis in EPR, J. Magn. Reson., 178, 42-55, https://doi.org/10.1016/j.jmr.2005.08.013, 2006.

Suter, D. and Álvarez, G. A.: Colloquium: Protecting quantum information against environmental noise, Rev.Mod. Phys., 88, 041001, 10.1103/RevModPhys.88.041001, 2016.

1 Tyryshkin, A. M., Tojo, S., Morton, J. J. L., Riemann, H., Abrosimov, N. V., Becker, P., Pohl, H.-J.,
2 Schenkel, T., Thewalt, M. L. W., Itoh, K. M., and Lyon, S. A.: Electron spin coherence exceeding
3 seconds in high-purity silicon, Nat. Mat., 11, 143-147, 10.1038/nmat3182, 2012.

4 Wang, G., Liang, X., Chen, L., Gao, Q., Wang, J.-G., Zhang, P., Peng, Q., and Xu, S.: Iridium-
5 Catalyzed Distal Hydroboration of Aliphatic Internal Alkenes, Angew. Chem. Intl. Ed., 58, 8187-
6 8191, https://doi.org/10.1002/anie.201902464, 2019.

7 Ward, R., Bowman, A., Sozudogru, E., El-Mkami, H., Owen-Hughes, T., and Norman, D. G.: EPR
8 distance measurements in deuterated proteins, J. Magn. Reson., 207, 164-167,
9 https://doi.org/10.1016/j.jmr.2010.08.002, 2010.

10 Wilson, C. B., Qi, M., Han, S., and Sherwin, M. S.: Gadolinium Spin Decoherence Mechanisms at
11 High Magnetic Fields, J. Phys. Chem. Lett., 14, 10578-10584, 10.1021/acs.jpclett.3c01847, 2023.

12 Wolfe, J. P.: Direct Observation of a Nuclear Spin Diffusion Barrier, Phys. Rev. Lett., 31, 907-910,
13 10.1103/PhysRevLett.31.907, 1973.

14 Yang, Y., Wang, J.-T., Pei, Y.-Y., and Su, X.-C.: Site-specific tagging proteins via a rigid, stable and
15 short thiolether tether for paramagnetic spectroscopic analysis, Chem. Comm., 51, 2824-2827,
16 10.1039/C4CC08493D, 2015.

17 Yang, Y., Yang, F., Li, X.-Y., Su, X.-C., and Goldfarb, D.: In-Cell EPR Distance Measurements on
18 Ubiquitin Labeled with a Rigid PyMTA-Gd(III) Tag, J. Phys.Chem.B, 123, 1050-1059,
19 10.1021/acs.jpcb.8b11442, 2019.

20